consideration, that maintenance of special conditions for superconductive magnet requires high additional expenses.

Currently in Tokyo Women's Medical University low magnetic field strength (0.3 Tesla) open intraoperative magnetic resonance imaging (iMRI) is used. As it was shown in the present study such system is useful for the resection of intracranial glioma. Moreover, our latest experience shows, that such MR scanner permits to obtain intraoperative diffusion-weighted images for the visualization of pyramidal tracts [22], as well as functional MR images for identification of the motor cortex. Using specially developed coils for the scanning of open brain surgery that provide higher signal-to-noise ratio, represents significant improvement of image quality, especially of contrast-enhanced tumours, which was reflected in a higher resection rate of such neoplasms as reported in the "study group". Novel organization of the neurosurgical operating theatre with low magnetic field strength iMRI permits to perform sophisticated procedures, using conventional surgical devices and instruments. Spatial separation of the operative table and MR gantry and removable head-holder coil provides freedom for any surgical manipulations, which can be done in both supine and prone position of the patient. Therefore, it seems that compared to other available systems our device can have the best cost-to-benefit ratio, if under "benefit" one will accept image quality and system effectiveness.

Extensive removal of glioma

The benefits of resective surgery in cases of glioma include relief of compression of the tumor bulk on the surrounding brain (important for neurological improvement), reduction of the volume of neoplasm (can render adjuvant therapy more effective), and precise histological diagnosis, which is important for the choice of optimal treatment strategy and prediction of prognosis. Many investigators have demonstrated the benefits of complete resection for low-grade gliomas [2, 5, 27], which is in complete agreement with our own experience. Moreover, while not sufficiently proved [12, 25], extensive removal of malignant glioma can improve patient prognosis. According to a retrospective analysis of the brain tumor registry of Japan [31], which included 6398 cases of malignant glioma from 281 different hospitals, survival was longer if total removal of tumor was achieved, compared to subtotal resection or biopsy alone. Similar results were reported by two recent, large, multi-center cooperative trials, in which identical treatment protocols were used. Overall, 6 prospective studies published from 1990 found significant correlation between resection rate of malignant glial tumors and patient survival [1, 7, 8, 14–16, 23]. Therefore, while further well-designed prospective studies on this topic will be needed in future, currently available data suggest that complete resection of glial neoplasms can be considered as a reasonable surgical goal.

Evaluation of residual tumor volume is not a simple task. Albert *et al.* [1] reported that the use of different methods for assessment of the resection rate could significantly influence results. Particularly, the resection rate estimated by the operating surgeon was significantly higher compared to postoperative CT or MRI. Still, there is no standard definition of "complete removal of glioma", which is reflected in the wide variation of reported total resection rates (from 6.2 to 71%) [6, 33]. It may be suspected that some of such cases represent nothing more than biopsy. Our method of post-operative evaluation of residual tumor volume based on the enhanced area of T_1-weighted MR images might be criticized, because autopsy specimens showed that glioblastoma cells can be identified even beyond hyperintense signal on T_2-weighted MR images. However, Wirtz *et al.* [35] and Lacroix *et al.* [17] in their clinical studies assessed the residual tumor in the same way as we did and showed its importance for the prediction of patient survival. For glioblastoma, a resection rate of 98% or greater can be considered as prognostically significant break-point.

Complications after resective surgery for gliomas

Neurological morbidity after resective surgery for gliomas varies from 6 to 28% [4, 34], and may be even higher in cases of recurrent tumors, especially if previous radiotherapy was effected [4]. Overall, 33 patients (34%) of the present series exhibited more or less prominent worsening of their pre-existing symptoms after removal of the brain tumor. Moreover, more aggressive tumor resection, as performed in the "study group", was associated with astatistically significant increase of temporary post-operative neurological deterioration.

Removal of tumors adjacent to the corona radiata and posterior limb of the internal capsule was associated with a higher incidence of neurological morbidity.

Our treatment algorithm, based on "update" neuronavigation, permitted precise orientation in the operative field with a minimal risk of mislocalization errors. Therefore, in our opinion, neurological deterioration encountered in some patients of the present series was mainly caused not by direct injury of the specific anatomical structures, which usually are clearly identified by neuronavigation and subcortical brain mapping, but due to compromise of their vascular supply. Anyway, removal of tumor located in the vicinity of the pyramidal tracts has to be considered high-risk surgery for post-operative neurological deterioration, even if the whole spectrum of the most sophisticated modern neurosurgical armamentarium, including iMRI, is available in the operating theatre.

It has to be noted that not one case of postoperative hemorrhage was found in the present series. Previous reports suggest that such complications occur at a rate of 2–3% after surgery for parenchymal brain tumors [4, 26]. It seems that aggressive tumor resection that can be achieved with the help of iMRI, permits to avoid a condition known as "hemorrhage in the residual tumor" or "wounded glioma syndrome". Additionally, despite relatively longer operative time, the rate of infectious complications in the present series (2%) did not differ from those in other reports.

Conclusions

The use of iMRI during surgery for intracranial gliomas allows identification of residual tumor and performing aggressive resection with good functional outcome. In 49% of cases of the present series total removal of the neoplasm was attained, with a mean resection rate of 93%. Surgical experience with the iMRI system, establishment of treatment algorithm, and improvement of image quality are of paramount importance for attainment of optimal results.

Acknowledgments

We thank Drs. Yoshikazu Okada, Ken'ichi Hirasawa, Masahiko Tanaka, and Kohsaku Amano (Department of Neurosurgery, Tokyo Women's Medical University), Makoto Ozaki, Minoru Nomura, Satoshi Nagata, Takayuki Kunisawa, and Kiyoshi Naemura (Department of Anesthesiology, Tokyo Women's Medical University), the scrub nurses and technical staff for tremendous help during surgical procedures with iMRI. We wish to express our gratitude to Takashi Sakayori, Madoka Sugiura, Hiroki Taniguchi, Kyojiro Nambu, Kouichi Suzukawa, and Yoshiyuki Fujita for their invaluable technical support. Drs. Nobuhiko Hata, Yuji Okawara, and Mikhail Chernov provided great assistance and made thoughtful suggestions during preparation of the manuscript. The present study was supported by the Industrial Technology Research Grant Program in 2000–2005 (A45003a) from the New Energy and Industrial Technology Development Organization of Japan to Yoshihiro Muragaki.

References

1. Albert FK, Forsting M, Sartor K, Adams HP, Kunze S (1994) Early postoperative magnetic resonance imaging after resection of malignant glioma: objective evaluation of residual tumor and its influence on regrowth and prognosis. Neurosurgery 34: 45–60
2. Berger MS, Deliganis AV, Dobbins J, Keles GE (1994) The effect of extent of resection on recurrence in patients with low grade cerebral hemisphere gliomas. Cancer 74: 1784–1791
3. Black PM, Moriarty T, Alexander E, Stieg P, Woodard EJ, Gleason PL, Martin CH, Kikinis R, Schwartz RB, Jolesz FA (1997) Development and implementation of intraoperative magnetic resonance imaging and its neurosurgical applications. Neurosurgery 41: 831–842
4. Brell M, Ibanez J, Caral L, Ferrer E (2000) Factors influencing surgical complications of intra-axial brain tumours. Acta Neurochir (Wien) 142: 739–750
5. Britton JW, Cascino GD, Sharbrough FW, Kelly PJ (1994) Low-grade glial neoplasms and intractable partial epilepsy: efficacy of surgical treatment. Epilepsia 35: 1130–1135
6. Ciric I, Rovin R, Cozzens JW, Eller TW, Vick NA, Mikhael MA (1990) Role of surgery in the treatment of malignant cerebral gliomas. Presented at Association of Neurological Surgeons, Park Ridge, IL
7. Curran WJ, Scott CB, Horton J, Nelson JS, Weinstein AS, Nelson DF, Fischbach AJ, Chang CH, Rotman M, Asbell SO (1992) Does extent of surgery influence outcome for astrocytoma with atypical or anaplastic foci (AAF)? A report from three Radiation Therapy Oncology Group (RTOG) trials. J Neurooncol 12: 219–227
8. Devaux BC, O'Fallon JR, Kelly PJ (1993) Resection, biopsy, and survival in malignant glial neoplasms. A retrospective study of clinical parameters, therapy, and outcome. J Neurosurg 78: 767–775
9. Fransson A, Andreo P, Potter R (2001) Aspects of MR image distortions in radiotherapy treatment planning. Strahlenther Onkol 177: 59–73
10. Gasser T, Ganslandt O, Sandalcioglu E, Stolke D, Fahlbusch R, Nimsky C (2005) Intraoperative functional MRI: implementation and preliminary experience. Neuroimage 26: 685–693
11. Hadani M, Spiegelman R, Feldman Z, Berkenstadt H, Ram Z (2001) Novel, compact, intraoperative magnetic resonance imaging-guided system for conventional neurosurgical operating rooms. Neurosurgery 48: 799–807
12. Hess KR (1999) Extent of resection as a prognostic variable in the treatment of gliomas. J Neurooncol 42: 227–231
13. Iseki H, Muragaki Y, Taira T, Kawamata T, Maruyama T, Naemura K, Nambu K, Sugiura M, Hirai N, Hori T, Takakura K (2001) New possibilities for stereotaxis. Information-guided stereotaxis. Stereotact Funct Neurosurg 76: 159–167
14. Kelly PJ, Hunt C (1994) The limited value of cytoreductive surgery in elderly patients with malignant gliomas. Neurosurgery 34: 62–66
15. Kiwit JC, Floeth FW, Bock WJ (1996) Survival in malignant glioma: analysis of prognostic factors with special regard to cytoreductive surgery. Zentralblatt fur Neurochirurgie 57: 76–88

16. Kreth FW, Warnke PC, Scheremet R, Ostertag CB (1993) Surgical resection and radiation therapy versus biopsy and radiation therapy in the treatment of glioblastoma multiforme. J Neurosurg 762–726
17. Laeroix M, Abi-Said D, Fourney DR, Gokaslan ZL, Shi W, DeMonte F, Lang FF, McCutcheon IE, Hassenbusch SJ, Holland E, Hess K, Michael C, Miller D, Sawaya R (2001) A multivariate analysis of 416 patients with glioblastoma multiforme: prognosis, extent of resection, and survival. J Neurosurg 95: 190–198
18. Muragaki Y, Iseki H, Kawamata T, Sugiura M, Amano K, Taira T, Hori T, Nambu K, Suzukawa K (2000) Development of "real-time" navigation system updated with intraoperative MR imaging for total removal of glioma. Funct Neurosurg (Japanese) 39: 80–81
19. Nimsky C, Ganslandt O, Cerny S, Hastreiter P, Greiner G, Fahlbusch R (2000) Quantification of, visualization, and compensation for brain shift using intraoperative magnetic resonance imaging. Neurosurgery 47: 1070–1080
20. Nimsky C, Ganslandt O, Hastreiter P, Wang R, Benner T, Sorensen AG, Fahlbusch R (2005) Intraoperative diffusion-tensor MR imaging: shifting of white matter tracts during neurosurgical procedures – initial experience. Radiology 234: 218–225
21. Nimsky C, Ganslandt O, Von Keller B, Romstock J, Fahlbusch R (2004) Intraoperative high-field-strength MR imaging: implementation and experience in 200 patients. Radiology 233: 67–78
22. Ozawa N, Muragaki Y, Shirakawa K, Suzukawa K, Nakamura R, Watanabe H, Iseki H, Takakura K (2004) Development of navigation system employing intra-operative diffusion weighted imaging using open MRI. In: Lemke HU, Vannier MW, Inamura A, Farman AG, Doi K, Reiber HC (eds) CARS2004 Computer assisted radiology and surgery. Elsevier, Amsterdam, pp 679–702
23. Prados MD, Gutin PH, Phillips TL, Wara WM, Larson DA, Sneed PK, Davis RL, Ahn DK, Lamborn K, Wilson CB (1992) Highly anaplastic astrocytoma: a review of 357 patients treated between 1977 and 1989. Int J Radiat Oncol Biol Phys 23: 3–8
24. Rubino GJ, Farahani K, McGill D, Van De Wiele B, Villablanca JP, Wang-Mathieson A (2000) Magnetic resonance imaging-guided neurosurgery in the magnetic fringe fields: the next step in neuronavigation. Neurosurgery 46: 643–653
25. Sawaya R (1999) Extent of resection in malignant gliomas: a critical summary. J Neurooncol 42: 303–305
26. Sawaya R, Hammoud M, Schoppa D, Hess KR, Wu SZ, Shi WM, Wildrick DM (1998) Neurosurgical outcomes in a modern series of 400 craniotomies for treatment of parenchymal tumors. Neurosurgery 42: 1044–1055
27. Scerrati M, Roselli R, Iacoangeli M, Pompucci A, Rossi GF (1996) Prognostic factors in low grade (WHO grade II) gliomas of the cerebral hemispheres: the role of surgery. J Neurol Neurosurg Psychiatry 61: 291–296
28. Shi WM, Wildrick DM, Sawaya R (1998) Volumetric measurement of brain tumors from MR imaging. J Neurooncol 37: 87–93
29. Steinmeier R, Fahlbusch R, Ganslandt O, Nimsky C, Buchfelder M, Kaus M, Heigl T, Lenz G, Kuth R, Huk W (1998) Intraoperative magnetic resonance imaging with the magnetom open scanner: concepts, neurosurgical indications, and procedures: a preliminary report. Neurosurgery 43: 739–747
30. Sutherland GR, Louw DF (1999) Intraoperative MRI: a moving magnet. CMAJ 161: 1293
31. The Committee of Brain Tumor Registry of Japan (2000) Report of brain tumor registry of Japan (1969–1993) 10th edition. Neurol Med Chir (Tokyo) [Suppl] 40: 1–106
32. Tronnier VM, Wirtz CR, Knauth M, Lenz G, Pastyr O, Bonsanto MM, Albert FK, Kuth R, Staubert A, Schlegel W, Sartor K, Kunze S (1997) Intraoperative diagnostic and interventional magnetic resonance imaging in neurosurgery. Neurosurgery 40: 891–900
33. Vecht CJ, Avezaat CJJ, van Putten WLJ, Eijkenboom WMH, Stefanko SZ (1990) The influence of the extent of surgery on the neurologic function and suvival in malignant glioma. A retrospective analysis in 243 patients. J Neurol Neurosurg Psychiatry 53: 466–471
34. Vives KP, Piepmeier JM (1999) Complications and expected outcome of glioma surgery. J Neurooncol 42: 289–302
35. Wirtz CR, Knauth M, Staubert A, Bonsanto MM, Sartor K, Kunze S, Tronnier VM (2000) Clinical evaluation and follow-up results for intraoperative magnetic resonance imaging in neurosurgery. Neurosurgery 46: 1112–1120
36. Wirtz CR, Tronnier VM, Bonsanto MM, Knauth M, Staubert A, Albert FK, Kunze S (1997) Image-guided neurosurgery with intraoperative MRI: update of frameless stereotaxy and radicality control. Stereotact Funct Neurosurg 68: 39–43

Correspondence: Y. Muragaki, Faculty of Advanced Techno-Surgery, Institute of Advanced Biomedical Engineering and Science, Graduate school of Medicine, Tokyo Women's Medical University 8-1 Kawada-cho, Shinjuku-ku, Tokyo, Japan 162-8666, e-mail: ymuragaki@nij.twmu.ac.jp

THE JOURNAL OF GENE MEDICINE
J Gene Med 2008; 10: 329–339.
Published online 28 January 2008 in Wiley InterScience (www.interscience.wiley.com) DOI: 10.1002/jgm.1160

RESEARCH ARTICLE

A phase I clinical trial of interferon-beta gene therapy for high-grade glioma: novel findings from gene expression profiling and autopsy

Toshihiko Wakabayashi[1]
Atsushi Natsume[2]
Yoshio Hashizume[3]
Masazumi Fujii[2]
Masaaki Mizuno[2]
Jun Yoshida[1,2]*

[1]*Center for Genetic and Regenerative Medicine, Nagoya University Hospital, 65 Tsurumai-cho, Showa-ku, Nagoya 466-8550, Japan*

[2]*Department of Neurosurgery, Nagoya University School of Medicine, 65 Tsurumai-cho, Showa-ku, Nagoya 466-8550, Japan*

[3]*Institute of Medical Science for Aging, Aichi Medical University, Nagakute, Aichi 480-1195, Japan*

*Correspondence to: Jun Yoshida, Department of Neurosurgery, Nagoya University School of Medicine, 65 Tsurumai-cho, Showa-ku, Nagoya 4668550, Japan.
E-mail:
nsoffice@med.nagoya-u.ac.jp

Received: 25 September 2007
Revised: 7 November 2007
Accepted: 27 November 2007

Abstract

Background High-grade gliomas are highly lethal neoplasms representing approximately 20% of all intracranial tumors. Cationic liposome-mediated interferon-beta (*IFN-β*) gene transfer has been found to induce regression of experimental glioma. We have previously performed a pilot clinical trial to evaluate the safety and effectiveness of this *IFN-β* gene therapy in five patients with high-grade glioma. Two patients showed more than 50% reduction while others had stable disease 10 weeks after treatment initiation.

Methods To identify alterations in gene expression in brain tumors 2 weeks after the gene therapy trial, we used a microarray technology and Gene Ontology analysis. The results were validated by patients' clinical course and findings of histology and autopsy.

Results and conclusions Using hierarchical clustering and principal component analysis, five series of gene therapy trials were classified according to the response to *IFN-β* gene therapy. Significant changes in gene expression related to immunoresponse and apoptosis were observed. Moreover, novel patterns of altered gene expression, such as inhibition of neovascularization, were identified, suggesting the involvement of pathways reported previously as not involved. Autopsy and histological examinations revealed dramatic changes in the tumor tissues after therapy in all patients. Many tumor cells showed necrotic changes, and immunohistochemistry identified numerous CD8-positive lymphocytes and macrophages infiltrating the tumor and surrounding tissues; these were probably the effects of therapy. Simultaneously, CD34-immunoreactive vessels were notably decreased in the vector-injected brain. This study facilitates the understanding of the antitumor mechanism and helps identify candidate target molecules for new approaches. However, additional clinical trials are warranted. Copyright © 2008 John Wiley & Sons, Ltd.

Introduction

Gliomas are the most common primary tumors of the central nervous system, accounting for 30% of adult primary brain tumors. The prognosis of patients with the advanced glioma, glioblastoma multiforme (GBM), is very poor, with a median survival of 8–10 months [1]. Similar to many malignant tumors, malignant gliomas including GBM have therapeutically intractable features related to its biology – characteristically high proliferation and highly invasive nature that prevent complete tumor resection and cause significant neurological morbidity and, ultimately, mortality.

Molecular neurosurgery with gene therapy has been investigated clinically since 1992 in an effort to overcome this formidable neoplasm [2]. These clinical trials mainly included two approaches: (a) suicide gene therapy using the herpes simplex virus-thymidine kinase (*HSV-tk*) gene along with the administration of gancyclovir (GCV) and (b) cytokine gene therapy [3].

We initiated the cytokine gene therapy wherein the interferon-beta (*IFN-β*) gene was delivered via cationic liposomes in 2000 based on the following preclinical and experimental studies. *In vitro* experiments demonstrated that cationic liposome-mediated human *IFN-β* gene transfer to cultured human glioma cells induced a cytocidal but not a cytostatic response even in IFN-resistant human glioma cell lines, probably involving apoptosis [4]. *In vivo* experiments using nude mice implanted with human glioma cells intracranially or subcutaneously revealed that the local administration of cationic liposomes containing the human *IFN-β* gene induced marked tumor growth reduction, prolonged survival, and natural killer (NK) cell activation [5,6]. In addition, a similar growth-inhibitory effect was also observed in a syngeneic intracranial mouse glioma model treated with the liposome-mediated murine *IFN-β* gene, and this gene therapy system induced specific cytotoxic T-cell immunity against mouse glioma and the NK cells [7,8].

IFN-β has been reported to exert pleiotropic biological effects [9]. Although identified and named for its ability to interfere with viral replication in treated cells, IFN-β has immunomodulatory and anti-proliferative effects. However, little is known regarding the mechanism of action of IFN-β that is overexpressed in human neoplasms. We have previously performed a pilot clinical trial of *IFN-β* gene therapy in five patients with malignant glioma [10]. In the present study, we performed a microarray analysis on tissue samples that were obtained before and after the *IFN-β* gene therapy from five patients with malignant glioma. We detected changes in gene expression that could be predicted based on previous studies, confirming the validity of the methods used. We also identified novel patterns of altered gene expression, suggesting the involvement of pathways that were previously considered as not involved in the response of gliomas to IFN-β. Finally, we validated the novel findings from microarray analysis by comparing them with the autopsy findings.

Materials and methods

Preparation of liposomes containing the human *IFN-β* gene plasmid

Clinical-grade liposomes were prepared at the Human Gene Therapy Vector-Producing Facility of Nagoya University. Equipment and procedures in the facility are sufficient to produce vectors in adequate quantities for clinical trials of gene therapy. The liposome preparation used in this study was a frozen concentrate of liposomes containing the human *IFN-β* gene (pDRSV-IFN-β). The pDRSV-IFN-β plasmid included an inserted human *IFN-β* gene driven by the Rous sarcoma virus (RSV) promoter. Prior to administration, the preparation was rapidly thawed and diluted to the desired concentration (30 μg of DNA/ml) with sterile phosphate-buffered saline.

Patients

The subjects (gene therapy cases from our previous study [10], GT1–5) were selected from among patients (age range 28–64 years) with recurrent malignant gliomas (GBM or anaplastic astrocytoma [AA]). All patients had undergone surgery and were diagnosed histologically with GBM or AA, according to the World Health Organization (WHO, Geneva, Switzerland) classification. All the patients had failed to respond to standard therapy including surgery, radiotherapy, chemotherapy, and immunotherapy. All the tumors were localized to the supratentorial compartment, without dissemination via the cerebrospinal fluid (CSF). Tumor progression was distinctly evident on sequential magnetic resonance (MR) images in all patients before their enrollment in the study. No patient had received prior anticancer therapy for at least 4 weeks.

Study design

The study design was described in the previous report [10]. Briefly, the initial treatment comprised tumor removal and injection of liposomes containing the human *IFN-β* gene into the margin of the resulting defect (day 0). Subsequent injection schedules were as follows: days 14, 17, 21, 24, and 28 (GT1) or days 14, 21, and 28 (GT2–5). The surgical margin of the resection cavity was infiltrated with 1 ml liposomes containing the human *IFN-β* gene at a DNA concentration of 30 μg/ml such that the preparation was evenly distributed among four sites. Each injection was administered over 5 min (50 μl/ min), using our original designed needle and a microsyringe pump. After injection, the needle was left in the brain for an additional 3 min and then slowly withdrawn. The subsequent injections on the later days were performed stereotactically under local anesthesia, delivering 15 μg (GT1) or 30 μg (GT2–5) of DNA; the same procedure was used after histologically confirming the presence of viable-appearing tumor cells. If such tumor cells could not be detected in any of the biopsy samples obtained from at least four sites, we did not inject the liposomes. Injection tracks were chosen so as to optimize coverage of the tumor based on its size, geometry, and location. The best response for each patient was derived from the objective tumor response according to the Response Evaluation Criteria in Solid Tumors (RECIST) [11]. Complete response was defined as the disappearance of the enhanced tumor over a period of not less than 4 weeks.

Partial response was defined as ≥70% decrease in the maximum diameter of the enhanced lesion. Stable disease was defined as <70% decrease or <20% increase in the maximum diameter of the enhanced lesion. Progressive disease was defined as ≥20% increase in the maximum diameter of the enhanced lesion or appearance of a new lesion. Survival was measured from day 1 of gene therapy until disease progression, or death.

Sampling

Tissue samples were obtained before injection from the injection site under a microscope during the first surgery. After the second surgery, samples were obtained using a stereotactic technique from the injection site. Tissue samples were immediately divided into two pieces. One was used for pathological assessment and the other was immediately frozen with liquid nitrogen and maintained at −140 °C until genetic analysis.

Tissue preparation and microarray analysis

RNA was isolated from 25–50 mg of tissue per sample. The standard Trizol preparation protocol (Invitrogen, Carlsbad, CA, USA) and reagents were used for total RNA isolation. RNA amplification and labeling were performed using the Amino Allyl MessageAmp aRNA kit (Ambion, Austin, TX, USA), as described previously [12]. Briefly, after reverse transcription reactions (2 μg total RNA per sample) had been performed, double-stranded cDNA was transcribed *in vitro* into amino allyl cRNA. The purified and concentrated cRNA (5 μg) was coupled with Cy3 or Cy5 dyes (GE Healthcare, Little Chalfont, UK). The fragmented cRNA was added to custom-made microarrays in a hybridization solution and then hybridized at 42 °C for 16 h. The oligonucleotide microarray was codeveloped with Ms. Yasuko Yoshida (NGK Insulators, Ltd., Nagoya, Japan). The slide contained 1500 human elements together with positive and negative controls (Supplementary Table S1, see Supplementary Material). Our microarray comprises functionally well-characterized genes involved in various important cellular processes, including the IFN-related pathway, apoptosis, cell cycle, transcription, immune function, and neural development. Moreover, our microarray is extremely suitable for studying the IFN-related pathway. Recently, we reported some IFN-related data obtained by using this custom-made oligonucleotide microarray for the study published [12]. Subsequently, the arrays were washed, scanned at 10 μm pixel size, gridded, and analyzed (GenePix 4000B; Axon Instruments, Union City, CA, USA). The background was subtracted, and the median sum and median ratio were calculated. Flagged spots and spots with a sum intensity (CH1 and CH2) of <100 AU were excluded. The data were normalized by trimmed mean at 10% to account for the differences in the amounts of labeled RNA or labeling efficiencies. The hierarchical cluster analysis and principal component analysis were performed using Acuity 4.0 software (Axon Instruments). The potential genes we selected on completion of the analysis were those whose expression changed by more than 2-fold. The lists of differently expressed genes were imported into MetaCore™ (GeneGO, St. Joseph, MI, USA), a web-based computational platform; this program automatically associates Gene Ontology (GO) terms from public databases to the submitted gene reporters. The number of differently expressed genes that represented specific GO nodes was statistically compared, and Bonferroni's correction was employed for multiple comparisons.

Real-time quantitative reverse-transcriptase polymerase chain reaction (real-time Q-RT-PCR)

Eleven genes from the microarray experiment were selected for validation by real-time Q-RT-PCR. Based on the results of GO analysis, we selected genes that were included in the four GO terms with a statistically significance ($p < 0.05$, i.e. apoptosis, immune response, angiogenesis and cell motility). cDNA was produced using the Transcriptor First Strand cDNA synthesis kit (Roche, Mannheim, Germany), according to the manufacturer's protocol. Quantitative mRNA levels were detected by the LightCycler real-time RT-PCR system (version 3.39) by using the LightCycler FastStart DNA Master SYBR Green I (Roche). The names and primer sequences of the selected genes are listed in Table 1. The threshold cycle (Ct), i.e., the cycle number at which the amount of the amplified gene of interest reaches a fixed threshold, was subsequently determined. The relative quantification was calculated using the comparative Ct method. The relative quantification value of the target normalized to an endogenous control *GAPDH* gene and relative to a calibrator is expressed as $2^{-\Delta\Delta Ct}$ (fold difference), where ΔCt = (the Ct of the target genes) − (the Ct of the *GAPDH* gene) and $\Delta\Delta Ct$ = (the ΔCt of the samples for the target genes) − (the ΔCt of the calibrator for the target genes).

Pathology

As a pathological assessment of tumor response, paraffin-embedded specimens were evaluated by routine hematoxylin and eosin staining and immunohistochemistry using the following anti-human antibodies: CD8 (C8/144B; Nichirei, Tokyo, Japan), CD68 (KP-1; Dako-Cytomation, Glostrup, Denmark), and CD34 (NU-4A1; Nichirei). CD34 has been most commonly used in studies of tumor angiogenesis. The detection of CD34 labeling has

Table 1. Primer sequences for real-time Q-RT-PCR

Gene name		Sequence
GAPDH	Forward	GACCACAGTCCATGCCATCAC
	Reverse	GTCCACCACCCTGTTGCTGTA
IkB	Forward	CACTTATGGACAACTATGAGGT CTCTGG
	Reverse	CTGTCTTGTGGACAACGCAGTGG AATTTTAGG
EFNB1	Forward	CCAATGCTGTGAGCCTGAG
	Reverse	CGAACAATGCCACCTTGGAGTTG
CASP4	Forward	GTTTTGGATAACTTGGTGGA
	Reverse	ATTGTGATTTCTGCCTCTGT
TSP-1	Forward	CCGGCGTGAAGTGTACTAGCTA
	Reverse	TGCACTTGGCGTTCTTGTT
IGFBP3	Forward	AACTGTGGCCATGACTGAGGA
	Reverse	CTCCCTGAGCCTGACTTTGC
GMCSF	Forward	GCCAGCCACTACAAGCAGCAC
	Reverse	CAAAGGGGATGACAAGCAGAAAG
TRAIL	Forward	CACATTGTCTTCTCCAAACTC
	Reverse	GTCCATGTCTATCAAGTGCTC
STAT1	Forward	AAGGTGGCAGGATGTCTCGTG
	Reverse	TGGTCTCGTGTTCTTCTGTTCTG
IL-8	Forward	CGATGTCAGTGCATAAAGACA
	Reverse	TGAATTCTCAGCCCTCTTCAAAAA
GADD45A	Forward	TGACTTTGGAGGAATTCTCGGC
	Reverse	ATGAATGTGGATTCGTCACCAG CACGCAGT
SCG2	Forward	AGGCCAAGCAAACAACAAG
	Reverse	CACCAAACTTCCTGCCATC

been interpreted as the presence of newly formed vessels in endothelial cells during angiogenesis. Apoptosis was detected using the TACS2 TdT Kit (Funakoshi, Tokyo, Japan).

Results

The overall clinical course of patients treated with *IFN-β* gene therapy

The safety evaluation and the interim clinical data of our clinical trial have been reported previously [10]. The overall clinical course of the patients treated with the *IFN-β* gene therapy is demonstrated in Table 2. After the first injection, GT1 (a 31-year-old female) and GT5 (a 28-year-old female) exhibited a stable disease, as determined by measuring the tumor by outlining the enhanced area on MR imaging. The disease changed only slightly over 10 weeks; however, the disease eventually progressed, and these patients died at 6 months and 11 months after treatment, respectively. On the other hand, GT2 (a 64-year-old female) and GT3 (a 54-year-old male) experienced a better response: the disease showed partial or complete regression over 15 months, and the patients could survive for more than 26 months. GT4 was excluded from evaluation because the pathological examination revealed no viable tumor cells in the formalin-fixed specimens of vector-injected sites, and no production of IFN-β was observed by either enzyme-immunoassay or RT-PCR. It has been reported that in patients with AA that recurred after prior radiotherapy and chemotherapy, the median progression-free survival (PFS) and median survival were 5.4 months and 13.6 months, respectively [13]. In our institution, we have previously reported that the median PFS and the median survival were 5.5 and 9.3 months, respectively, for patients with recurrent AA [14]. Although this phase I clinical trial included only five patients, mean PFS and survival in this study were 9 ± 2.7 and 17 ± 4.5 months, respectively. Comparatively, our results suggest that *IFN-β* gene therapy may be effective in glioma patients in whom prior treatment has failed to produce a response. The present study provides foundation for a phase II trial of *IFN-β* gene therapy.

Table 2. Clinical courses of patients treated with *IFN-β* gene therapy

Patient	Age/Sex	Pathology	Best response	PFS (months)	OS (months)
GT1	31/F	GBM	SD	3	6
GT2	64/F	AA	PR	16	29
GT3	54/M	AA	CR	15	26
GT4	48/M	AA	SD	6	13
GT5	28/F	AA	SD	5	11
Mean ± SE				9 ± 2.7	17 ± 4.5

PFS: progression-free survival (the time from day 1 of gene therapy to disease progression)
OS: overall survival (the time from day 1 of gene therapy to death)
GT: gene therapy case number, F: female, M: male, GBM: glioblastoma multiforme, AA: anaplastic astrocytoma
SE: standard error
CR: complete response, PR: partial response, SD: stable disease. The definitions are described in the text.

Cluster and principal component analyses exhibit a correlation with the efficacy of *IFN-β* gene therapy

First, to test the quality of our custom-made microarray technique, we employed the RNA extracted from the tumor tissue of GT1 before and after the *IFN-β* gene therapy to generate the scatter plots shown in Figure 1A. A pre-treatment versus (vs.) pre-treatment (self-on-self) comparison of probes yielded a correlation coefficient of 0.9997, while the pre-treatment vs. post-treatment comparison of probes yielded a value of 0.9557. Thus, the almost absence of scatter in the self-on-self comparison was validated. Unsupervised hierarchical cluster analysis and principal component analysis were performed for the five patients (GT1–5) receiving the *IFN-β* gene therapy (Figure 1B). Pearson correlation-based algorithm and Euclidean distance were applied based on the similarity in the expression pattern across all probe sets. The pattern of expression changes between pre- and post-treatment in GT2 resembled that in GT3. Subsequently, gene expression changes obtained from GT5 were very similar to those of the cluster comprising GT2 and GT3, followed by GT1. GT4 was the most distinct from the others: it was an exceptional case because no production of IFN-β was observed after the *IFN-β* gene transfer. Collectively, the cluster analysis of the expression pattern exhibited good

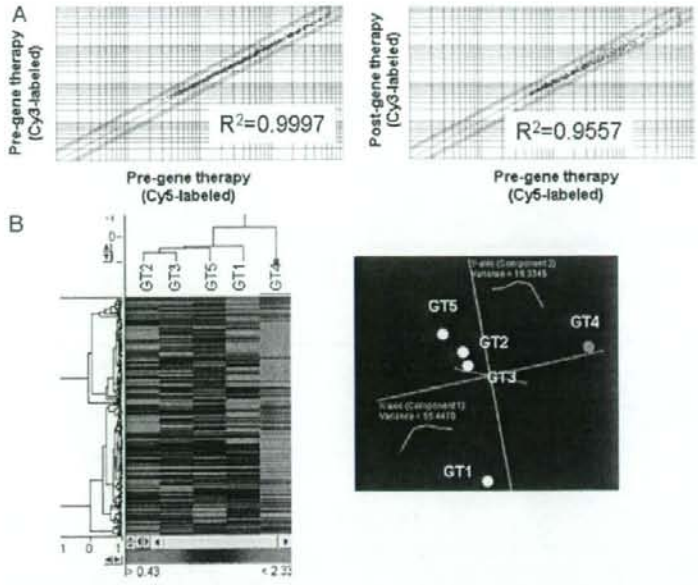

Figure 1. (A) Quality control of our custom-made microarray technique. We employed the RNA extracted from the tumor tissue of patient 1 (GT1) before and after the *IFN-β* gene therapy to generate the scatter plots. A pre-treatment versus (vs.) pre-treatment (self-on-self) comparison of probes yielded a correlation coefficient of 0.9997 (left), while the pre-treatment vs. post-treatment comparison of probes yielded a value of 0.9557 (right). (B) Unsupervised hierarchical cluster analysis (left) and principal component analysis (right) were performed for the five patients (GT1–5) receiving the *IFN-β* gene therapy. Pearson correlation-based algorithm and Euclidean distance were applied based on the similarity in the expression pattern across all probe sets. The pattern of expression changes between pre- and post-treatment in GT2 resembled that in GT3. Subsequently, gene expression changes obtained from GT5 were very similar to those of the cluster comprising GT2 and GT3, followed by GT1. GT4 was the most distinct from the others

similarity to the response of the patients treated with the *IFN-β* gene therapy.

Identification of differentially expressed genes after *IFN-β* gene therapy

To identify the differentially expressed genes after *IFN-β* gene therapy, we selected potential genes whose expression changed by more than 2-fold in all the patients except GT4. A total of 21 genes that fulfilled our criteria were upregulated while eight genes were downregulated following the *IFN-β* gene therapy (Tables 3 and 4). To identify the biological processes significantly involved in *IFN-β* gene transfer ($p < 0.05$), the identified genes were then processed through the Gene Ontology (GO) program. The majority of the differentially expressed genes were related to biological processes such as apoptosis (programmed cell death), immune response, angiogenesis, and cell motility (Table 5). We selected genes that were categorized in these significant processes, namely, caspase 4 (CASP4), gadd45, insulin-like growth factor-binding protein 3 (IGFBP3), IkB, Apo2-ligand (TRAIL), STAT1, GMCSF, IL8, thrombospondin1 (TSP1), serectogranin II (SCG2), and ephrin-B1 (EFNB1). We then validated the expression changes between pre- and post-*IFN-β* gene therapy by real-time Q-RT-PCR. As shown in Figure 2, we could show the marked upregulation of CASP4, GADD45, IkB, TRAIL, STAT1, GMCSF, IL8, TSP1, and SCG2, and the marked downregulation of IGFBP3 and EFNB1. Based on the GO-derived biological process of individual genes, the *IFN-β* gene therapy appeared to possess the biological activity to induce apoptosis and immune response and suppress angiogenesis.

Pathological changes following *IFN-β* gene therapy reflect gene expression patterns

Pathological assessments revealed dramatic changes in the tumor tissues after gene therapy in all patients except GT4. Pleomorphic tumor cells with marked nuclear atypia and brisk mitotic activity were observed even before the *IFN-β* gene therapy; however, they developed necrotic changes over time (Figures 3A–3C). TUNEL staining demonstrated a number of apoptotic cells in the vector-injected tumoral area (Figure 3D). Immunohistochemistry identified predominantly CD8-positive lymphocytes and CD68-positive macrophages infiltrating the tumor and surrounding tissues (Figures 3E and 3F). The CD4-positive T cells and CD20-positive B cells were observed in negligible amounts (data not

Table 3. Upregulated genes by *IFN-β* gene therapy

Mean fold change	Gene name	Symbol	GenBank ID	GO biological process
2.018	Eukaryotic translation initiation factor 2-alpha kinase 2	EIF2AK2	M35663	regulation of transcription, DNA-dependent, translation, protein amino acid phosphorylation, apoptosis, virus-infected cell apoptosis
2.089	Thrombospondin 1	THBS1	NM_003246	cell motility, inflammatory response, cell adhesion, multicellular organismal development, nervous system development
2.117	Erythroblastosis virus oncogene homolog 2	ETS-2	J04102	skeletal development, regulation of transcription (DNA-dependent)
2.129	MHC class I HLA-C allele	HLA-C	M11886	ciliary or flagellar motility, antigen processing and presentation of peptide antigen via MHC class I, immune response, antigen processing and presentation
2.173	Retinoblastoma binding protein 2	RBBP2	S66431	transcription, regulation of transcription (DNA-dependent), transcription from RNA polymerase II promoter, positive regulation of transcription
2.250	Activating transcription factor 3	ATF3	L19871	gluconeogenesis, transcription, regulation of transcription (DNA-dependent)
2.278	Secretogranin II	SCG2	M25756	MAPKKK cascade, angiogenesis, negative regulation of endothelial cell proliferation, cell motility, inflammatory response
2.329	Caspase 4	CASP4	NM_001225	proteolysis, induction of apoptosis, regulation of apoptosis
2.490	Cysteine protease	ICErel-II	U28014	proteolysis, induction of apoptosis, regulation of apoptosis
2.500	Nuclear factor of kappa light polypeptide gene enhancer in B-cells inhibitor, alpha	NFKBIA	M69043	protein import into nucleus, translocation, apoptosis, cytoplasmic sequestering of NF-kappaB, regulation of cell proliferation, regulation of NF-kappaB import into nucleus
2.643	Heme oxygenase	HMOX1	X06985	heme oxidation, positive regulation of I-kappaB kinase/NF-kappaB cascade, response to stimulus
2.667	Growth arrest and DNA-damage-inducible protein (Gadd153)	GADD153	S40706	regulation of progression through cell cycle, transcription, regulation of transcription, DNA-dependent, response to DNA damage stimulus, ER overload response
2.803	Major histocompatibility complex, class I, B	HLA-B	NM_005514	antigen processing and presentation of peptide antigen via MHC class I, defense response, immune response, antigen processing and presentation
3.009	Pro-cathepsin L	CTSL1	X12451	proteolysis
3.243	Granulocyte-macrophage colony stimulating factor	GMCSF	M11220	immune response, cellular defense response, cell surface receptor linked signal transduction, multicellular organismal development, positive regulation of cell proliferation
4.193	Interferon induced transmembrane protein 3	IFITM3	NM_021034	immune response, response to biotic stimulus
4.415	Growth arrest and DNA-damage-inducible protein (gadd45)	GADD45A	M60974	regulation of progression through cell cycle, regulation of cyclin-dependent protein kinase activity, DNA repair, negative regulation of protein kinase activity, apoptosis
4.557	Apo-2 ligand (TRAIL)	APO2L	U57059	apoptosis, induction of apoptosis, immune response, signal transduction, cell-cell signaling
8.626	Signal transducer and activator of transcription 1	STAT1	M97936	regulation of progression through cell cycle, transcription, regulation of transcription, DNA-dependent, transcription from RNA polymerase II promoter, caspase activation
15.932	Monocyte-derived neutrophil chemotactic factor	IL-8	Y00787	angiogenesis, cell motility, chemotaxis, inflammatory response, immune response

Mean fold change is expressed as the average of fold changes of gene expression in all the patients except GT4.
The source of Gene Ontology (GO) biological process: MetaCore™

shown). These findings were almost identical in all patients; therefore, it was believed that they represented the therapeutic effect.

After obtaining consent, we examined the brain of GT2 who died 29 months after *IFN-β* delivery (Figure 4A). A recurrence of malignant glioma was confirmed, with tumor cells invading the midbrain (Figures 4B and 4D). However, the specimen obtained from the vector-injected area displayed robust necrosis with a large area of hyaline-like degeneration (Figure 4C). Immunostaining with anti-CD34 antibody demonstrated few capillaries in the vector-injected area, while there

Table 4. Downregulated genes by *IFN-β* gene therapy

Mean fold change	Gene name	Symbol	GenBank ID	GO biological process
0.174	Matrix Gla protein	MGP	NM_000900	cartilage condensation, ossification, multicellular organismal development, sensory perception of sound, cell differentiation
0.185	Connective tissue growth factor	CTGF	NM_001901	cartilage condensation, ossification, angiogenesis, regulation of cell growth, DNA replication
0.365	Jagged 1	JAG1	U61276	angiogenesis, cell fate determination, morphogenesis of an epithelial sheet, cell communication, Notch signaling pathway
0.365	Myristoylated alanine-rich protein kinase C substrate	MARCKS	NM_002356	cell motility
0.391	Ephrin-B1	EFNB1	U09304	neural crest cell migration, cell adhesion, cell-cell signaling, multicellular organismal development, nervous system development, cell motility
0.464	Insulin-like growth factor-binding protein	IGFBP3	M31159	regulation of cell growth, negative regulation of signal transduction, positive regulation of apoptosis, positive regulation of myoblast differentiation
0.499	Nuclear receptor co-repressor 2	NCOR2	U37146	regulation of transcription, DNA-dependent, negative regulation of transcription, negative regulation of transcription, DNA-dependent

Mean fold change is expressed as the average of fold changes of gene expression in all the patients except GT4.
The source of Gene Ontology (GO) biological process: MetaCore™

Table 5. Significant Gene Ontology (GO) terms of differentially expressed genes following *IFN-β* gene therapy

GO term	*p*-value
Apoptosis	0.00221
Immune response	0.00231
Angiogenesis	0.0315
Cell motility	0.0448

The lists of differently expressed genes were imported into MetaCore ™; this program automatically associates GO terms from public databases to the submitted gene reporters. The number of differently expressed genes that represented specific GO nodes was statistically compared, and Bonferroni's correction was employed for multiple comparisons.

were a larger number of CD34-positive vessels within the tumor (Figures 4E and 4F). Taken together, there were significant pathological changes that are related to the induction of immune response and apoptosis and inhibition of vascularization. These findings were in good agreement with our microarray data.

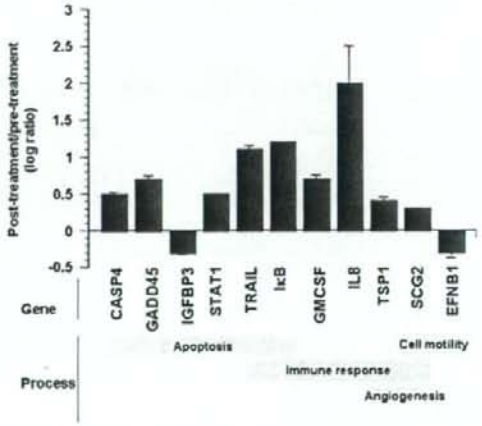

Figure 2. Validation of microarray data. We selected 11 genes that were categorized in significant processes (apoptosis, immune response, angiogenesis and cell motility), then validated the expression changes by real-time Q-RT-PCR. Values are expressed as log ratio of the post-treatment gene expression normalized to the *GAPDH* gene relative to the pre-treatment gene expression. Non-abbreviated gene names are described in Tables 3 and 4

Discussion

In this communication, we have reported that the changes in gene expression patterns in the microarray were correlated with the clinical course of the patients treated with *IFN-β* gene therapy. We also identified significant genes that were differentially expressed after the *IFN-β* gene delivery. A majority of these genes were closely related to apoptosis, immune response, and angiogenesis, and we confirmed the findings by real-time Q-RT-PCR and immunohistochemical studies with tissues obtained before and after treatment and at autopsy. The induction of apoptosis and immune response was consistent with our previous studies that were performed in glioma cell lines and orthotopic animal models. A noteworthy finding of this study is that the liposome-mediated *IFN-β* gene delivery appears to have an antiangiogenic effect; this was not addressed in our previous studies. Here, we review our current and previous studies, related literature, and canonical pathway maps in MetaCore.

Induction of apoptosis

Previously, we have demonstrated that *IFN-β* gene transfer induces a substantial cytocidal response in human

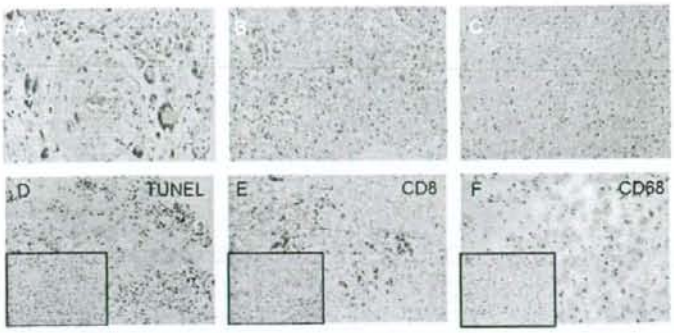

Figure 3. (A–C) Hematoxylin-eosin staining of the vector-injected site: (A) day 0; (B) day 17; and (C) day 28. Pleomorphic tumor cells with marked nuclear atypia and brisk mitotic activity were observed before the *IFN-β* gene therapy (A); however, they developed necrotic changes over time. (D) TUNEL staining on day 21 after gene therapy. Note a number of apoptotic cells in the vector-injected tumoral area. (E) CD8 immunohistochemistry on day 21 after gene therapy. (F) CD68 immunohistochemistry on day 21 after gene therapy. Sister sections as in (D–F), stainings before gene therapy

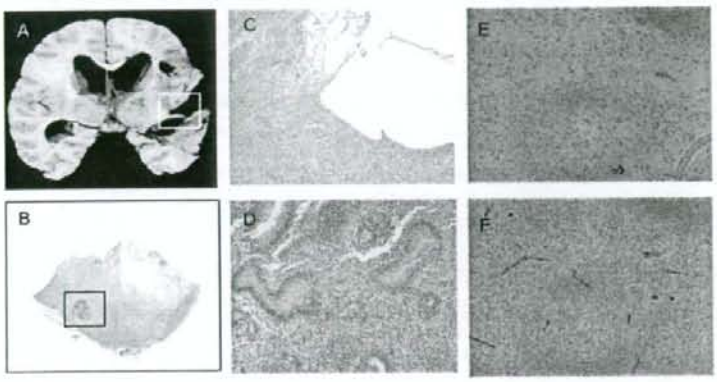

Figure 4. (A) The brain of patient 2 including the vector-injected area (a coronal section). (B) The midbrain invaded by tumor cells. (C) A representative hematoxylin-eosin stained section of the vector-injected area (a high-magnification image of the boxed area in (A)). It displays robust necrosis with a large area of hyaline-like degeneration. (D) A high-magnification image of the boxed area in panel B. (E, F) Immunostainings of the vector-injected area (E) and the tumoral area (F) in the autopsied brain (29 months after gene therapy) with anti-CD34 antibody

glioma and renal cell carcinoma cells by involving apoptosis [4,15]. In animal models, the growth of such tumors was markedly inhibited after treatment with cationic liposomes containing the *IFN-β* gene [6]. Interestingly, cationic liposome-mediated *IFN-β* gene transfer induced apoptosis in cultured neoplasm cells that are resistant to the IFN-β protein. Indeed, the histological examination in this clinical trial revealed robust TUNEL-positive cells on day 21 after the *IFN-β* gene therapy and morphological changes showing necrosis/hyaline-like degeneration in the vector-injected site in the autopsied brain. Figure 5 summarizes the molecular mechanism of apoptosis induced by cationic liposome-mediated *IFN-β* gene delivery based on current and previous evidence. Primarily, IFN-β transduces its signal via the classical Janus-activated kinase (JAK)/signal transducer and activator of transcription (STAT) phosphorylation cascades [9]. Local and profound exposure of glioma cells to IFN-β that can be achieved by vector-mediated production appears to correlate with a significant prolongation of the JAK/STAT pathway phosphorylation. This apoptotic process seemingly is dependent not on caspase-3 or caspase-8 activation and cleavage of DEF45/ICAD, but on the activation of caspase-7 and DNase γ [16]. Besides the caspase cascade, the microarray and the following GO analyses displayed the upregulation of GADD45, IkB, and TNF-related apoptosis-inducing ligands (TRAIL or APO2-L) and the downregulation of IGFBP3. There is evidence that IFN-β induces p53 expression in human cancers [12,17], and GADD45 is involved in the p53-dependent apoptotic pathway by binding to the proliferating cell nuclear antigen (PCNA) and affecting PCNA interaction with some cyclin-dependent kinase (CDK) complexes [18,19]. TRAIL is one of the TNF super family cytokines; it binds to death receptor (DR)-4 and DR5 and induces apoptosis via the

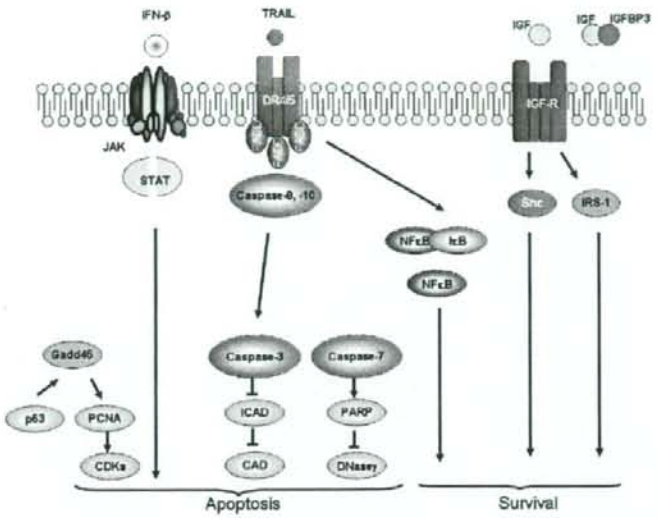

Figure 5. Gene network of differentially expressed apoptosis-related genes following *IFN-β* gene therapy. The network was illustrated by reviewing our current and previous studies, related literature, and canonical pathway maps in MetaCore™

recruitment of its adaptor protein, Fas-associated death domain (FADD), and through the activation of caspases [20,21]. IkB/nuclear factor (NF)-kB is known to be involved in the TNF family-mediated signal transductions. In resting cells, NF-kB dimers are sequestered in the cytoplasm in an inactive form via association with IkB. Phosphorylation, ubiquitination, and subsequent degradation of IkB lead to the translocation of NF-kB to the nucleus [22,23]. There is growing evidence that NF-kB is involved in the regulation of apoptosis [24,25]. Although its role appears to tend toward either the proapoptotic or antiapoptotic pathway, aberrant IkB/NF-kB balancing may be its critical function in apoptosis. IGF signaling was another intriguing pathway detected in this study. IGF exerts potent mitogenic and differentiating effects on most cell types. IGF that binds to the receptor activates the receptor kinase, and through initial tyrosine phosphorylation reactions, the IGF signals are transduced to complex networks that are ultimately responsible for cell proliferation, modulation of tissue differentiation, and protection from apoptosis [26]. IGFBP3 prolongs the half-life of IGF and has been shown to inhibit the growth-promoting effects of IGF [27].

Since the proteins/genes playing a role in the abovementioned apoptosis-related pathways are partly overlapped, it remains unclear whether these pathways are mutually correlated or independent. However, evidence clearly shows that the *IFN-β* gene therapy trial induced apoptosis in glioma.

Induction of immune response

In the current study, we detected an increased expression of GMCSF and IL-8 in the glioma tissues of patients receiving the *IFN-β* gene, and thus demonstrated that *IFN-β* gene therapy appears to facilitate immune cell infiltration comprising CD8-positive T cells and CD68-positive macrophages in the brain tumor. In our previous studies using a syngeneic orthotopic mouse glioma model treated with the murine *IFN-β* gene, we have shown that the activation of cellular immunity participates in antitumor effects in addition to direct apoptosis [7,8]. GMCSF is a well-known cytokine that stimulates the growth and differentiation of hematopoietic precursor cells to various lineages, including granulocytes, macrophages, eosinophils, and erythrocytes. In addition, its critical function to promote the maturation and differentiation of dendritic cells has been widely utilized to generate strong antigen-presenting cells in vaccine therapy for a variety of cancers [28,29]. IL-8 is a chemotactic factor that attracts neutrophils, basophils, and T cells but not monocytes. It is also involved in neutrophil activation [30]. Recently, Yeh *et al.* reported an increase in IL-8 synthesis by STAT activation [31]. These findings suggest IFN-*β* as one of the most potent molecules for augmenting tumor immunity following gene transfer into glioma cells.

Inhibition of angiogenesis

GBMs are one of the most highly vascularized malignant tumors. Neovascularization in tumors is correlated with their biological aggressiveness, degree of malignancy, and clinical recurrence [32]. In fact, microvascular hyperplasia is one of the pathological criteria used to distinguish a high-grade glioma. Therefore, research and therapy strategies have focused on understanding the mechanism leading to the origin of tumor angiogenic

blood vessels in order to block angiogenesis and tumor progression. Angiogenesis is tightly regulated and maintained by a fine balance between factors that act as stimulators or repressors and by a dynamic crosstalk between a tumor and the tumor microenvironment. Besides endothelial cells, several types of cells participate directly or indirectly in tumor neovascularization. Glioma cells, pericytes, leukocytes, and bone-marrow-derived endothelial progenitors play a role in angiogenesis. Because of its complexity, we were unable to address this issue in the experiments of cell culture and animal models, although IFNs are highly pleiotropic cytokines also endowed with a marked antiangiogenic activity [33]. In the present study involving the examination of the clinical samples including tumor cells and of the microenvironment after *IFN-β* gene transfer, for the first time, we could demonstrate an antiangiogenic phenotype induced by *IFN-β*. This immunohistochemical study with CD34 labeling revealed few capillaries in the vector-injected area, while there were a larger number of CD34-positive vasculatures in the tumor. The detection of CD34 labeling has been interpreted as the presence of newly formed vessels in endothelial cells during angiogenesis. Molecular signature by microarray analysis detected a significant upregulation of TSP-1, a potent angiogenesis inhibitor; however, we believe that other molecules are probably involved via subtle tuning [34,35].

Future directions

Based on the final clinical course of the patients treated with the *IFN-β* gene therapy, the findings presented in this communication suggest that *IFN-β* gene therapy may be effective in glioma patients who have not responded to prior treatment, although this phase I clinical trial comprised only five patients. This study provides the foundation for a phase II trial of *IFN-β* gene therapy. In addition, the experience gathered in the developmental and review processes of this clinical trial may contribute to the development of other advanced medicines. The understanding of the antitumor mechanism facilitates the identification of candidate target molecules for new approaches.

Supplementary material

The supplementary electronic material for this paper is available in Wiley InterScience at: http://www.0interscience.wiley.com/jpages/1099-498X/suppmat/.

Acknowledgements

The first author [T.W.] received the 2007 JSGT (The Japan Society of Gene Therapy) Award for presentation of this work. This work was supported by a Grant-in-Aid for Scientific Research (B) (No. 18390395) from the Ministry of Health, Labor, and Welfare and by the Japan Society for the Promotion of Science, Tokyo.

References

1. Fine HA, Dear KB, Loeffler JS, *et al.* Meta-analysis of radiation therapy with and without adjuvant chemotherapy for malignant gliomas in adults. *Cancer* 1993; **71**: 2585–2597.
2. Culver KW, Ram Z, Wallbridge S, *et al.* In vivo gene transfer with retroviral vector-producer cells for treatment of experimental brain tumors. *Science* 1992; **256**: 1550–1552.
3. http://www.wiley.co.uk/genetherapy/clinical/.
4. Mizuno M, Yoshida J, Sugita K, *et al.* Growth inhibition of glioma cells transfected with the human beta-interferon gene by liposomes coupled with a monoclonal antibody. *Cancer Res* 1990; **50**: 7826–7829.
5. Yagi K, Hayashi Y, Ishida N, *et al.* Interferon-beta endogenously produced by intratumoral injection of cationic liposome-encapsulated gene: cytocidal effect on glioma transplanted into nude mouse brain. *Biochem Mol Biol Int* 1994; **32**: 167–171.
6. Mizuno M, Yoshida J. Effect of human interferon beta gene transfer upon human glioma, transplanted into nude mouse brain, involves induced natural killer cells. *Cancer Immunol Immunother* 1998; **47**: 227–232.
7. Natsume A, Mizuno M, Ryuke Y, *et al.* Antitumor effect and cellular immunity activation by murine interferon-beta gene transfer against intracerebral glioma in mouse. *Gene Ther* 1999; **6**: 1626–1633.
8. Natsume A, Tsujimura K, Mizuno M, *et al.* IFN-beta gene therapy induces systemic antitumor immunity against malignant glioma. *J Neurooncol* 2000; **47**: 117–124.
9. Borden EC, Lindner D, Dreicer R, *et al.* Second-generation interferons for cancer: clinical targets. *Semin Cancer Biol* 2000; **10**: 125–144.
10. Yoshida J, Mizuno M, Fujii M, *et al.* Human gene therapy for malignant gliomas (glioblastoma multiforme and anaplastic astrocytoma) by in vivo transduction with human interferon beta gene using cationic liposomes. *Hum Gene Ther* 2004; **15**: 77–86.
11. Therasse P, Arbuck SG, Eisenhauer EA, *et al.* New guidelines to evaluate the response to treatment in solid tumors. European Organization for Research and Treatment of Cancer, National Cancer Institute of the United States, National Cancer Institute of Canada. *J Natl Cancer Inst* 2000; **92**: 205–216.
12. Natsume A, Ishii D, Wakabayashi T, *et al.* IFN-beta down-regulates the expression of DNA repair gene MGMT and sensitizes resistant glioma cells to temozolomide. *Cancer Res* 2005; **65**: 7573–7579.
13. Stupp R, Reni M, Gatta G, *et al.* Anaplastic astrocytoma in adults. *Crit Rev Oncol Hematol* 2007; **63**: 72–80.
14. Ishii D, Natsume A, Wakabayashi T, *et al.* Efficacy of temozolomide is correlated with 1p loss and methylation of the deoxyribonucleic acid repair gene MGMT in malignant gliomas. *Neurol Med Chir (Tokyo)* 2007; **47**: 341–349; discussion 350.
15. Nakanishi H, Mizutani Y, Kawauchi A, *et al.* Significant antitumoral activity of cationic multilamellar liposomes containing human IFN-beta gene against human renal cell carcinoma. *Clin Cancer Res* 2003; **9**: 1129–1135.
16. Saito R, Mizuno M, Hatano M, *et al.* Two different mechanisms of apoptosis resistance observed in interferon-beta induced apoptosis of human glioma cells. *J Neurooncol* 2004; **67**: 273–280.
17. Takaoka A, Hayakawa S, Yanai H, *et al.* Integration of interferon-alpha/beta signalling to p53 responses in tumour suppression and antiviral defence. *Nature* 2003; **424**: 516–523.
18. Smith ML, Chen IT, Zhan Q, *et al.* Interaction of the p53-regulated protein Gadd45 with proliferating cell nuclear antigen. *Science* 1994; **266**: 1376–1380.
19. Chung HK, Yi YW, Jung NC, *et al.* CR6-interacting factor 1 interacts with Gadd45 family proteins and modulates the cell cycle. *J Biol Chem* 2003; **278**: 28079–28088.
20. Pitti RM, Marsters SA, Ruppert S, *et al.* Induction of apoptosis by Apo-2 ligand, a new member of the tumor necrosis factor cytokine family. *J Biol Chem* 1996; **271**: 12687–12690.

21. Kischkel FC, Lawrence DA, Chuntharapai A, *et al.* Apo2L/TRAIL-dependent recruitment of endogenous FADD and caspase-8 to death receptors 4 and 5. *Immunity* 2000; **12**: 611–620.
22. Baldwin AS Jr. The NF-kappa B and I kappa B proteins: new discoveries and insights. *Annu Rev Immunol* 1996; **14**: 649–683.
23. Chen FE, Ghosh G. Regulation of DNA binding by Rel/NF-kappaB transcription factors: structural views. *Oncogene* 1999; **18**: 6845–6852.
24. de Martin R, Schmid JA, Hofer-Warbinek R. The NF-kappaB/Rel family of transcription factors in oncogenic transformation and apoptosis. *Mutat Res* 1999; **437**: 231–243.
25. Aggarwal BB. Apoptosis and nuclear factor-kappa B: a tale of association and dissociation. *Biochem Pharmacol* 2000; **60**: 1033–1039.
26. Laviola L, Natalicchio A, Giorgino F. The IGF-I signaling pathway. *Curr Pharm Des* 2007; **13**: 663–669.
27. Santer FR, Bacher N, Moser B, *et al.* Nuclear insulin-like growth factor binding protein-3 induces apoptosis and is targeted to ubiquitin/proteasome-dependent proteolysis. *Cancer Res* 2006; **66**: 3024–3033.
28. Dranoff G. GM-CSF-based cancer vaccines. *Immunol Rev* 2002; **188**: 147–154.
29. Eager R, Nemunaitis J. GM-CSF gene-transduced tumor vaccines. *Mol Ther* 2005; **12**: 18–27.
30. Xie K. Interleukin-8 and human cancer biology. *Cytokine Growth Factor Rev* 2001; **12**: 375–391.
31. Yeh M, Gharavi NM, Choi J, *et al.* Oxidized phospholipids increase interleukin 8 (IL-8) synthesis by activation of the c-src/signal transducers and activators of transcription (STAT)3 pathway. *J Biol Chem* 2004; **279**: 30175–30181.
32. Leon SP, Folkerth RD, Black PM. Microvessel density is a prognostic indicator for patients with astroglial brain tumors. *Cancer* 1996; **77**: 362–372.
33. Fidler IJ. Regulation of neoplastic angiogenesis. *J Natl Cancer Inst Monogr* 2001; 10–14.
34. Ren B, Yee KO, Lawler J, *et al.* Regulation of tumor angiogenesis by thrombospondin-1. *Biochim Biophys Acta* 2006; **1765**: 178–188.
35. Kargiotis O, Rao JS, Kyritsis AP. Mechanisms of angiogenesis in gliomas. *J Neurooncol* 2006; **78**: 281–293.

Int. J. Cancer: **122**, 2542–2553 (2008)

The DNA demethylating agent 5-aza-2′-deoxycytidine activates NY-ESO-1 antigenicity in orthotopic human glioma

Atsushi Natsume[1]*, Toshihiko Wakabayashi[1,2], Kunio Tsujimura[3]*, Shinji Shimato[1], Motokazu Ito[1], Kiyotaka Kuzushima[3], Yutaka Kondo[4], Yoshitaka Sekido[4], Hitomi Kawatsura[1], Yuji Narita[5] and Jun Yoshida[1,2]

[1]*Department of Neurosurgery, Nagoya University School of Medicine, Nagoya, Japan*
[2]*Center for Genetic and Regenerative Medicine, Nagoya University Hospital, Nagoya, Japan*
[3]*Division of Immunology, Aichi Cancer Center Research Institute, Nagoya, Japan*
[4]*Division of Molecular Oncology, Aichi Cancer Center Research Institute, Nagoya, Japan*
[5]*Department of Tissue Engineering, Nagoya University School of Medicine, Nagoya, Japan*

Cancer/testis antigens (CTAs) are considered to be suitable targets for the immunotherapy of human malignancies. It has been demonstrated that in a variety of tumors, the expression of certain CTAs is activated *via* the demethylation of their promoter CpG islands. In our study, we have shown that while the composite expression of 13 CTAs in 30 human glioma specimens and newly established cell lines from the Japanese population was nearly imperceptible, the DNA-demethylating agent 5-aza-2′-deoxycytidine (5-aza-CdR) markedly reactivated CTA expression in glioma cells but not in normal human cells. We quantified the diminished methylation status of NY-ESO-1-one of the most immunogenic CTAs-following 5-aza-CdR treatment by using a novel Pyrosequencing™ technology and methylation-specific PCR. Microarray analysis revealed that 5-aza-CdR is capable of signaling the immune system, particularly, human leukocyte antigen (HLA) class I upregulation. ^{51}Cr-release cytotoxicity assays and cold target inhibition assays using NY-ESO-1-specific cytotoxic T lymphocyte (CTL) lines demonstrated the presentation of *de novo* NY-ESO-1 antigenic peptides on the cell surfaces. In an orthotopic xenograft model, the systemic administration of 5-aza-CdR resulted in a significant volume reduction of the transplanted tumors and prolonged the survival of the animals after the adoptive transfer of NY-ESO-1-specific CTLs. These results suggested that 5-aza-CdR induces the expression of epigenetically silenced CTAs in poorly immunogenic gliomas and thereby presents a new strategy for tumor immunotherapy targeting 5-aza-CdR-induced CTAs.

Key words: glioma; cancer-testis antigens; DNA methylation; immunotherapy; NY-ESO-1

Over the last decade, there has been major progress in the identification and characterization of human tumor antigens recognized by the host immune system. A subgroup of tumor antigens, commonly referred to as cancer/testis antigens (CTAs), are expressed only in the tissues of the testis, ovary and placenta under normal conditions, but are also expressed in various types of human tumors.[1,2] Since normal CTA-expressing tissues do not express major histocompatibility complex (MHC) class I molecules, CD8 T cells cannot recognize CTAs expressed on these tissues, suggesting that CTAs are the ideal targets for tumor immunotherapy. CTAs and genes were originally identified through a variety of methods. These include T-cell epitope labeling,[3] serological analysis of cDNA expression libraries (SEREX),[4,5] differential gene expression analysis[6] and bioinformatics methods.[7–9] In particular, NY-ESO-1 is the most immunogenic CTA discovered thus far, and it is considered to be a highly promising therapeutic target for immunotherapy.[10] To date, very little is known regarding the physiological function(s) of these antigens or the mode in which the expression of their gene families is regulated.

Epigenetic alterations, including hypermethylation of promoter CpG islands, histone deacetylation of tumor suppressor and tumor-related genes,[11–13] and global DNA hypomethylation,[14,15] have been recognized as important contributors to carcinogenesis in humans. Global DNA hypomethylation has been observed in various neoplasms and is considered to occur at the early stages of tumor development.[16–18] However, it has been shown that the expression of certain CTA genes is reactivated in cancerous cells; this could be due to a loss of epigenetic regulation as observed when methylated chromatin regions are demethylated or when deacetylated histones are acetylated.[19] Therefore, recent evidence shows that the deregulation of the DNA methylation apparatus that occurs during cancer development could provide new therapeutic targets for cancer treatment.

The DNA demethylating agent 5-aza-2′-deoxycytidine (5-aza-CdR, decitabine) is a cytosine analogue that is incorporated into DNA during replication. It covalently binds DNA methyltransferase and inhibits its activity, leading to genome-wide demethylation.[20–24] There have been several studies demonstrating the ability of 5-aza-CdR to activate the gene expression of CTAs *in vitro* and *in vivo*, which may be silenced by the hypermethylation of their promoters. This drug has been used in clinical studies for the treatment of chronic myelogenous leukaemia (CML), sickle cell anaemia and myelodysplastic syndrome (MDS).[20,25–27] Previous evidence has clearly defined the epigenetic regulatory role of DNA methylation in the constitutive expression of CTAs by cutaneous melanoma cells and renal cancer cells and has demonstrated that *in vitro* treatment with 5-aza-CdR upregulated their expression in neoplastic cells.[28,29]

Gliomas are the most common primary tumors of the central nervous system; they account for 30% of adult primary brain tumors. Brain tumors remain difficult to cure despite recent advances in surgical, radiotherapeutic and chemotherapeutic approaches. In particular, there is currently no optimal treatment for glioblastoma multiforme, the most common malignant brain tumor in adults, and patients typically survive for a period less than a year. The poor outcome partly relates to the inability in delivering chemotherapeutic agents through the blood–brain barrier (BBB) and the low effect of radiation on the tumor. Therefore, new and more effective strategies are urgently required. Of these, the establishment of immunotherapy specifically targeting malignant cells is expected to improve tumor prognosis. It has recently been demonstrated that malignant glioma cells express certain known tumor-associated antigens such as HER-2, gp100, MAGE-

This article contains supplementary material available via the Internet at http://www.interscience.wiley.com/jpages/0020-7136/suppmat.

Grant sponsor: Grant-in-Aid for Scientific Research (B) from the Ministry of Health, Labor, and Welfare; Grant number: 18390395; Grant sponsor: the Japan Society for the Promotion of Science, Tokyo; Grant sponsor: the Third Team Comprehensive Control Research for Cancer from the Ministry of Health, Labor, and Welfare, Japan; Grant number: 26.

Kunio Tsujimura's current address is: Department of Infectious Diseases, Hamamatsu University School of Medicine, 1-20-1 Handa-yama, Higashi-ku, Hamamatsu 431-3192, Japan.

***Correspondence to:** Department of Neurosurgery, Nagoya University School of Medicine, 65 Tsurumai-cho, Showa-ku, Nagoya 466-8550, Japan. E-mail: anatsume@med.nagoya-u.ac.jp or ktsujimu@hama-med.ac.jp

Received 5 July 2007; Accepted after revision 4 December 2007
DOI 10.1002/ijc.23407
Published online 31 January 2008 in Wiley InterScience (www.interscience.wiley.com).

Publication of the International Union Against Cancer

1 and IL-13 receptor α2.[30–37] However, CTA profiling of glioma cells, in particular, in the Asian population remains unknown.

In our study, we analyzed the expression of 13 CTA genes (*MAGE-1*, *MAGE-3*, *MAGE-4*, *MAGE-6*, *MAGE-10*, *MAGE-3/6*, *LAGE-1*, *CT7*, *SCP-1*, *SSX-1*, *SSX-2*, *SSX-4* and *NY-ESO-1*) in 30 glioma tissues, 5 human glioma cell lines and 3 newly established cell lines from the Japanese population. Subsequently, the role of 5-aza-CdR in the regulation of the expression of various CTAs in glioma cells was analyzed. Finally, we demonstrated that NY-ESO-1, one of the most antigenic CTAs, is effectively induced in human glioma cells by 5-aza-CdR, and that these glioma cells forcibly expressing NY-ESO-1 show *in vitro* and *in vivo* sensitivity to NY-ESO-1-specific cytotoxic T lymphocytes (CTLs). Our present study provides the basis to establish novel immunotherapeutic approaches in glioma patients.

Material and methods

Cells

The human glioma cell lines U251 (human leukocyte antigen (HLA)-A2), SKMG1 (HLA-A24), AO2 (HLA-A3), U87MG (HLA-A2) and T98 (HLA-A2) were obtained from the Memorial Sloan-Kettering Cancer Institute (New York, NY) and maintained in Eagle's minimal essential medium (MEM) at 37°C in a humidified atmosphere of 5% CO_2 in air. A human osteosarcoma cell line, namely, SaOS-2 (NY-ESO-1+, HLA-A2), was kindly provided by Dr. Y. Nishida (Department of Orthopaedics, Nagoya University, Nagoya, Japan) and maintained in Dulbecco's modified Eagle's medium (DMEM; Nissui, Tokyo, Japan). A human myeloid leukaemia cell line K562 and the HLA-A*0201-transfected T2 cell line (T2.A2) were maintained in RPMI 1640 (Invitrogen, Carlsbad, CA). The medium was supplemented with 10% fetal bovine serum (FBS), 5 mM L-glutamine, 2 mM nonessential amino acids, and antibiotics (100 U/ml penicillin and 100 μg/ml streptomycin). Commercially available normal human astrocytes (NHA; Cambrex, Baltimore, MD) maintained in AGM medium with BulletKit supplement (Cambrex), human aortic smooth muscle cells (AoSMC; Cambrex), human adult fibroblasts (NHDF-ad; Cambrex) maintained in DMEM with 10% FBS, and human epidermal keratinocytes (NHEK, Kurabo, Osaka, Japan) maintained in Epilife medium (Cascade Biologics, Nottinghamshire, UK) supplemented with HuMedia-KG (Kurabo) were used as normal cells.

Reagents and peptides

A vial containing 5 mg lyophilized powder of 5-aza-CdR was obtained (Sigma-Aldrich, St. Louis, MO). The vial was reconstituted with 20 ml sterile water to obtain a 1 mM solution, and it was stocked at 4°C. The HLA-A2-binding NY-ESO-1 peptide, p157-165 (SLLMWITQC), which was initially identified using the T-cell line NW38-IVS-1[38] and the HLA-A2-binding IL-13Rα2 peptide, p345-354 (WLPFGFILI), which was identified previously,[37] was synthesized by Thermo Electron GmbH (>90% purity) (Ulm, Germany), and solubilized in 50% dimethyl sulphoxide (DMSO)/water.

Collection of surgical specimens

Thirty tumor samples were collected at the Nagoya University School of Medicine from patients whose tumors were histologically diagnosed as gliomas (WHO Grade II, III and IV). Genetic analysis in our study was approved by the ethical committee of Nagoya University Hospital. All patients provided written informed consent. All tissues were frozen immediately and stored at −80°C until use.

Primary-culture cells derived from patients with high-grade gliomas

Tumor tissues were derived from 3 patients with high-grade gliomas who had undergone surgical resection in Nagoya University Hospital, Nagoya, Japan; the tissues were primary-cultured as follows. Immediately after the brain tumors were removed from the patients, the tissues were homogenized and digested with 1% DNase and 0.1% trypsin for 30 min at 37°C and centrifuged at 800 rpm for 5 min. The cells were seeded at a density of 2×10^6 cells per 100-mm dish and maintained in DMEM supplemented with 10% FBS, 5 mM L-glutamine, 2 mM nonessential amino acids, and antibiotics (100 U/ml penicillin and 100 μg/ml streptomycin). The cells were then incubated in a standard tissue culture incubator (100% relative humidity and 5% CO_2). After achieving 80–90% confluence, they were subcultured onto a new 100-mm plate at a density of 2×10^6. The established cell lines were designated as NNS-10, NNS-11 and NNS-12. All cells were immunocytochemically confirmed as glioma cells based on their expression of glial-fibrilliary acidic protein (GFAP).

In vitro *treatment of cultured cells with 5-aza-CdR*

Treatment with 5-aza-CdR was performed as described in a previous study.[29] Cells were seeded at a density of 1.0×10^5 cells/well in a 6-well plate, and placed at 37°C overnight in a 5% CO_2 incubator. The next day, the cell culture medium was replaced with fresh medium containing 0.1, 1 and 10 μM 5-aza-CdR. The medium was changed every 12 hr for 2 days. The plates were wrapped in aluminum foil to avoid light exposure. At the end of the treatment, the medium was replaced with fresh medium without 5-aza-CdR, and the cells were cultured for an additional 48 hr.

RNA extraction

RNA was isolated from 25 to 50 mg of tissue/sample by using Trizol (Invitrogen) according to the manufacturer's protocol. RNA was finally resuspended in nuclease-free water.

Conventional reverse transcription PCR

cDNA was synthesized from 1 μg total RNA by using random hexamers and the Superscript II reverse transcription (RT) kit (Invitrogen), according to the manufacturer's protocol. For each PCR, 2 μl cDNA was used in a 20-μl reaction volume containing 200 mM dNTPs, 1 mM sense and antisense primers, 1.25 mM $MgCl_2$, 2 μl 10× PCR buffer, and 0.5 U Taq polymerase (Applied Biosystems, Foster City, CA). The PCR primers used were those listed in the Ref. 39 β-actin was used as the endogenous control. The cycling parameters were as follows: denaturation at 95°C for 45 s, primer annealing at 55°C for 45 s, and 35 cycles of extension at 72°C for 60 s. PCR cycling was preceded by an initial denaturation at 95°C for 5 min, followed by final extension at 72°C for 5 min. The PCR products were analyzed by electrophoresis on a 1.5% agarose gel; this was followed by staining with ethidium bromide. If no signal was observed, the remaining PCR products were amplified by an additional 15 cycles and analyzed again to confirm the absence of the signal.

Quantitative RT-PCR for NY-ESO-1 expression

After synthesis of the first cDNA strand as described earlier, quantitative RT-PCR was performed on the LightCycler real-time RT-PCR system (version 3.39) (Roche, Mannheim, Germany), using the FastStart Taqman Probe Master (ROX) (Roche) along with sets of primers and Universal ProbeLibrary probes (Roche) designed online with ProbeFinder version 2.40 (Roche). Probes specific for NY-ESO-1 were as follows: forward primer: 5′-TGTCCGGCAACATACTGACT-3′, reverse primer: 5′-ACTGCGTGATCCACATCAAC-3′, and Universal ProbeLibrary probe Human No. 67 (Roche), which yields a 111-nt amplicon. The endogenous reference gene *GAPDH* was amplified by the forward primer: 5′-AGCCACATCGCTCAGACAC-3′, reverse primer: 5′-CGCCCAATACGACCAAATC-3′, and Universal ProbeLibrary probe Human No. 60, which yields a 67-nt amplicon. Each sample was amplified as follows: 1 cycle at 95°C for 10 min followed by 40 cycles at 95°C for 15 s and 60°C for 1 min. cDNA from SaOS-2 was used to generate the standard curves for *NY-*

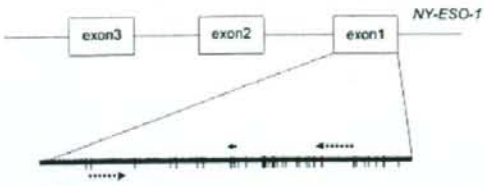

FIGURE 1 – Schematic view of the *NY-ESO-1* gene region analyzed in this study. Vertical lines indicate CpG dinucleotides, the solid arrow indicates the Pyrosequencing primer, and the broken arrows indicate the location of MSP primers.

ESO-1 and *GAPDH*. Standardization of samples was achieved by dividing the copy number of the target gene *NY-ESO-1* by that of the *GAPDH* gene. Values were expressed as ratios relative to *NY-ESO-1* expression in SaOS-2.

Western blot analysis

Cells treated with 5-aza-CdR (1 μM) and untreated cells were lysed in a buffer containing protease inhibitors. Protein samples (45 μg) were denatured at 100°C for 5 min and subsequently applied to each well and electrophoresed on a 12.5% polyacrylamide gel. After transferring the proteins to a polyvinylidene difluoride (PVDF) membrane, it was blocked with 3% low-fat skim milk, incubated with a monoclonal antibody (mAb) against NY-ESO-1 (ES121; Zymed, San Francisco, CA), and then washed and incubated with an horseradish peroxidase (HRP)-labelled secondary Ab. Visualization was performed using an enhanced chemiluminescence technique.

NY-ESO-1 promoter DNA methylation analyses

Methylation-specific PCR (MSP)[40] and Pyrosequencing™ technology[41] were used to determine the methylation status of the CpG island region of *NY-ESO-1*. None of the sequences identified in the *NY-ESO-1* promoter region fulfilled the criteria for CpG islands (length, >200 bp, G + C content, >50%, observed CpG/expected CpG ratio, ≥0.6).[42] The CpG islands and the location of the primers in exon 1 for DNA methylation analyses are shown in Figure 1. Genomic DNA isolation and sodium bisulphite conversion were performed as described previously.[43] The primer sequences and annealing temperatures of MSP were as reported previously.[44] The primer sequences for Pyrosequencing™ were designed using PSQ Assay Design (Biotage, Uppsala, Sweden). A 50-μl PCR was carried out in 60 mM Tris ± HCl (pH 8.5), 15 mM ammonium sulphate, 2 mM $MgCl_2$, 10% DMSO, 1 mM dNTP mix, 1 U Taq polymerase, 5 pmol forward primer (5′-GGGTTGAATGGATGTTGTAG-3′), 50 pmol reverse primer (5′-CRCCACCAAAACTATCAA-3′), 50 pmol biotinylated universal primer (5′- GGGACACCGCTGATCGTTTACRCCACCAAAAC-TATCAA-3′) and ~50 ng bisulphite-treated genomic DNA. The forward primer contains a 20-bp linker sequence on the 5′ end that is recognized by biotin-labeled primera; thus, the final PCR product can be purified using Sepharose beads. PCR cycling conditions were as follows: 95°C for 30 s, 60°C for 45 s and 72°C for 45 s for 55 cycles. The biotinylated PCR product was purified and made single-stranded to act as a template in a pyrosequencing reaction using the Pyrosequencing Vacuum Prep Tool (Pyrosequencing, Westborough, MA), as recommended by the manufacturer. In brief, the PCR product was bound to Streptavidin Sepharose HP (Amersham Biosciences, Uppsala, Sweden), and the Sepharose beads containing the immobilized PCR product were purified, washed, denatured using 0.2 M NaOH solution and washed again. Then, 0.3 mM pyrosequencing primer (5′-TGAATGGATGTTG-TAGATG-3′) was annealed to the purified single-stranded PCR product, and pyrosequencing was performed using the PSQ HS 96Pyrosequencing System (Pyrosequencing). Methylation quantification was performed using the provided software.

Flow cytometric analysis

Glioma cells were treated with 5-aza-CdR as described earlier. The treated and untreated cells were stained with anti-HLA class-I mAbs (W6/32; kindly provided by Dr. K. Itoh, Kurume University, Kurume, Japan) or isotype control mouse IgG2a followed by staining with fluoroscein isothiocyanate (FITC)-labelled anti-mouse IgG Abs. Flow cytometric analysis of stained cells was performed by using FACS Calibur (Becton Dickinson, San Jose, CA).

Induction of HLA-A2-restricted NY-ESO-1-specific CTL lines by peptide-pulsed dendritic cells

Peripheral blood mononuclear cells (PBMCs) from healthy volunteers genetically typed as HLA-A2-positive by SRL, (Tokyo, Japan) were isolated using Ficoll-Paque (Amersham Biosciences). Peptide-pulsed dendritic cells (DCs) were prepared from donor-derived PBMCs, as described previously[37] with minor modifications. In brief, the plastic adherent cells from PBMCs were cultured in AIM-V medium (Life Technologies, Gaithersburg, MD) supplemented with recombinant human granulocyte/macrophage-colony stimulating factor (rhGM-CSF, 500 U/ml) and rhIL-4 (500 U/ml) at 37°C in a humidified CO_2 (5%) incubator. After 6 days, the culture medium was removed, and the immature DCs were cultured in AIM-V supplemented with rhGM-CSF (500 U/ml), recombinant human interleukin (rhIL)-4 (500 U/ml), rhIL-6 (1,000 U/ml), recombinant human tumor necrosis factor-α (10 ng/ml), and IL-1β (10 ng/ml). All cytokines used were purchased from Strathmann Biotech AG, Hanover, Germany. Mature DCs were harvested after another 2 days, resuspended in AIM-V medium at 1×10^6 cells/ml with the peptide (10 μg/ml), and incubated for 4 hr at 37°C. The peptide-pulsed DCs were then treated with mitomycin-C, washed, and finally resuspended in AIM-V medium supplemented with 10% human AB serum. Autologous $CD8^+$ T cells were enriched from PBMCs by using magnetic microbeads (Miltenyi Biotech, Auburn, CA) and were added (1×10^6/well) to the peptide-pulsed DCs (1×10^5/well) in 2 ml AIM-V medium supplemented with 10% human AB serum, 1,000 U/ml rhIL-6, and 10 ng/ml rhIL-12 in each well of 24-well tissue culture plates. On day 7, the lymphocytes were restimulated with mitomycin-C-treated autologous DCs pulsed with peptides in AIM-V medium supplemented with 10% human AB serum, rhIL-2 and rhIL-7 (10 U/ml each). One week later and on a weekly basis thereafter, the responder cells were restimulated with peptide-pulsed DCs in a medium supplemented with rhIL-2 and rhIL-7 (10 U/ml each). The induction of NY-ESO-1-specific CTL lines was attempted 3 times.

CTL assay

The susceptibility of the untreated and 5-aza-CdR-treated U251 glioma cells (HLA-A2) to HLA-A2-restricted NY-ESO-1-specific CTL lines was evaluated by a standard 4-h ^{51}Cr-releasing assay at various (effector:target) E:T ratios. The percentage specific lysis was calculated as follows: 100 × (experimental release − spontaneous release)/(maximum release − spontaneous release).

Cold target inhibition assay

The cold target inhibition assay was performed as described previously.[45] In brief, T2.A2 cells were incubated with the NY-ESO-1 peptide or the irrelevant IL-13Rα2 peptide at a concentration of 10 μM for 1 hr. After extensive washing, the indicated numbers of peptide-loaded cells were incubated with 2×10^4 cytotoxic effector cells for 1 hr, and then 2×10^3 ^{51}Cr-labeled, 5-aza-CdR-treated U251 glioma cells were added to each well. Cytotoxicity was assessed at the E:T ratio of 10:1 as described earlier.

TABLE I – RT-PCR ANALYSIS FOR EXPRESSION OF CANCER-TESTIS ANTIGENS IN GLIOMA TISSUES

Patient	Pathology	NY-ESO-1	MAGE-1	MAGE-3	MAGE-4	MAGE-6	MAGE-10	MAGE-3/6	LAGE-1	CT7	SCP-1	SSX-1	SSX-2	SSX-4
1	GBM		■											
2	GBM													
3	GBM													
4	GBM													
5	GBM							■						
65	GBM													
184	GBM													
195	GBM													
197	GBM													
198	GBM													
199	GBM													
6	AA													
7	AA													
8	AA													
9	AA													
12	AA	■	■				■	■						
14	AA				■									
67	AA													
69	AA													
78	AA													
189	AA													
190	AA													
202	AA													
203	AA													
16	AS													
17	AS													
18	AS													
192	AS													
193	AS													
200	AS													
Rate		(1/30)	(2/30)	(0/30)	(1/30)	(0/30)	(1/30)	(2/30)	(0/30)	(0/30)	(0/30)	(0/30)	(0/30)	(0/30)

We investigated the composite expression of 13 CTAs in 30 human glioma specimens by RT-PCR analysis. MAGE-4, MAGE-10 and NY-ESO-1 were expressed in only 1 sample out of 30, and MAGE-1 and MAGE3/6 were expressed in 2 samples. Other CTAs were all negative in the 30 brain tumor specimens tested. The expression pattern of these did not correlate with the histological grades of gliomas.

Black and white boxes indicate positive and negative expression, respectively.

GBM, glioblastoma multiforme (WHO Grade IV); AA, anaplastic astrocytoma (Grade III); AS, astrocytoma (Grade II).

Orthotopic glioma xenograft model

Female nonobese diabetic/severe combined immunodeficiency disease (NOD/SCID) mice aged 5 weeks were used in the experiments. All mice were purchased from SLC, Hamamatsu, Japan. They were maintained under specific pathogen-free conditions in the animal facility of Nagoya University School of Medicine. Animal experiments were performed according to the principles enunciated in the Guide for the Care and Use of Laboratory Animals prepared by the Office of the Prime Minister of Japan.

Mice were anaesthetized with an intraperitoneal injection of pentobarbital (60–70 mg/kg body weight). After shaving the hair and incising the scalp, a burr hole was made in the skull 3 mm lateral to the midline and 4 mm posterior to the bregma using a dental drill. The head of each mouse was fixed in a stereotactic apparatus with ear bars, and 2×10^5 U251 cells in 2 μl PBS were stereotactically injected over 4 min at a depth of 2 mm below the dura mater. A sterile Hamilton syringe fitted with a 26-gauge needle was used with a microsyringe pump. The needle was retained in the brain for an additional 2-min duration and then slowly withdrawn.

To test the induction of *NY-ESO-1* in orthotopic glioma xenografts, 5-aza-CdR [0.2 mg/kg, intraperitoneally (i.p)] was administered every 12 hr for 4 consecutive days (8 pulses) starting on day 14 after glioma inoculation. The control brain tumor model was treated under similar experimental conditions by an i.p. PBS injection. To determine whether the treated cells upregulated the *NY-ESO-1* expression, the mice were killed on day 3 after the final 5-aza-CdR injection. The brain tumors were removed for RT-PCR for NY-ESO-1.

Tumor-inoculated NOD/SCID mice were randomly divided into 4 treatment groups (10 animals each) to examine the treatment efficacy of NY-ESO-1-specific CTLs in combination with 5-aza-CdR. The animals in the various groups were then injected as follows: Group I, PBS (i.p., 8 pulses starting from the day after tumor inoculation) and PBS (2 μl) intratumorally (i.t.) 6 days after tumor inoculation; Group II, PBS i.p. (8 pulses) and bulk CTLs (i.t., 1×10^6 cells/mouse in 2 μl); Group III, 5-aza-CdR i.p. (0.2 mg/kg, 8 pulses) and PBS (i.t., 2 μl); Group IV, 5-aza-CdR i.p. (0.2 mg/kg, 8 pulses) and bulk CTLs (i.t., 1×10^6 cells/mouse in 2 μl). Five mice in each group were euthanized using CO_2 inhalation on day 21 after tumor injection. The mice were transcardially perfused with 4% paraformaldehyde. The brain tissue was postfixed overnight, embedded in paraffin, and then cut into 5-μm serial horizontal sections. Tissue sections were stained by the standard haematoxylin and eosin technique. The growth inhibitory effect was evaluated by measuring the long (a) and short (b) axes in the coronal section showing the maximal area of each tumor. The approximate volume of the tumor (V) was calculated according to the formula, V (mm^3) = $a \times b^2/2$. In addition, the survival times of all the remaining mice were recorded.

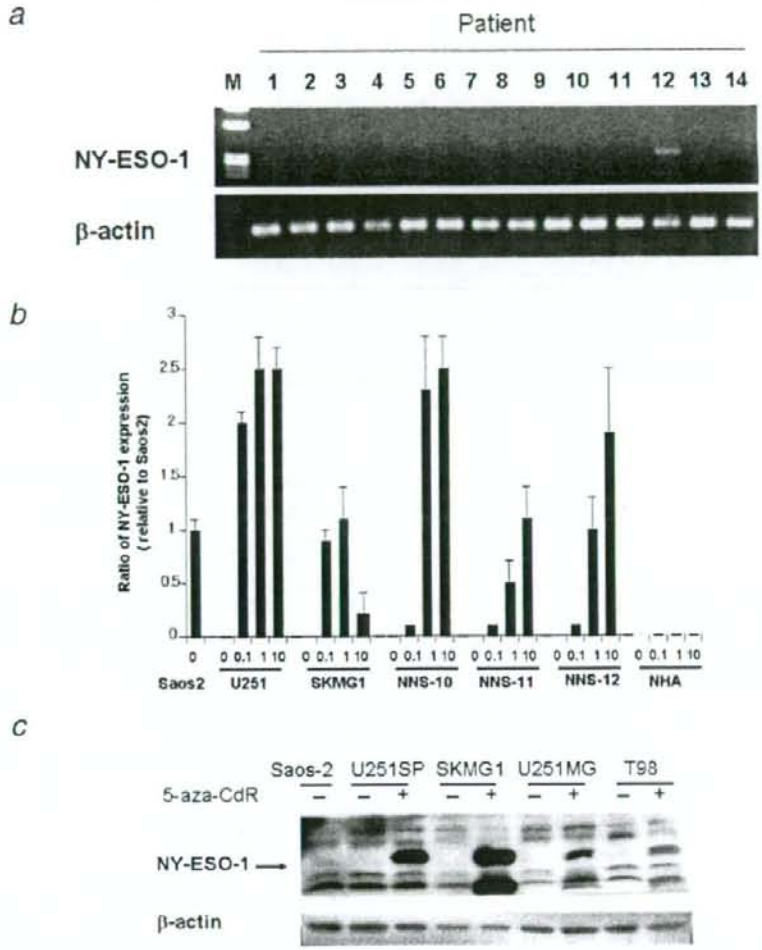

FIGURE 2 – *NY-ESO-1* expression in human gliomas. (*a*) RT-PCR for *NY-ESO-1* in surgical specimens of gliomas. The summarized data is presented in Table I. (*b*) Real-time quantitative RT-PCR showing *NY-ESO-1* induction in glioma cells but not in normal cells by 5-aza-CdR. The expression of *NY-ESO-1* was upregulated in U251, SKMG1, and primary-cultured glioma cells (NNS-10, NNS-11 and NNS-12) treated with 0.1, 1 and 10 μM 5-aza-CdR but not in normal astrocytes (NHA). 5-aza-CdR (10 μM) induced toxicity in SK-MG-1, leading to decreased *NY-ESO-1* expression. (*c*) Detection of NY-ESO-1 in glioma cell lines by western blot analysis. We prepared cell lysates of the untreated (−) gliomas (U251 (sublines SP and MG), SKMG1 and T98) and those treated (+) with 5-aza-CdR (1 μM) and *NY-ESO-1*-positive osteosarcomas (SaOs-2, as a positive control); western blotting analysis was conducted using an anti-NY-ESO-1 mAb.

The statistical significance of the difference in tumor volumes and Kaplan–Meier survival curves was determined by analysis of variance (ANOVA) (StatView, SAS Institute, Cary, NC) with Bonferroni's correction for multiple comparisons and the log-rank test (StatView), respectively.

Results

Expression of individual CTA genes in human gliomas and glioma cell lines

Although the expression frequencies of many CTAs in a variety of neoplasms have been determined, their expression in human gliomas remains unclear, and the expression frequency of CTAs varies drastically among ethnic groups.[39] It would be useful to analyze the expression pattern of CTAs in gliomas in the Japanese population. In our study, RT followed by 35 cycles of amplification revealed that the expression of CTA genes was nearly imperceptible in human gliomas, and the expression pattern of these genes did not correlate with the histological grades of the gliomas (Table I). *MAGE-4*, *MAGE-10* and *NY-ESO-1* were expressed in only 1 of 30 samples, and *MAGE-1* and *MAGE-3/6* were expressed in 2 samples. The samples were negative for *MAGE-3*, *MAGE-6*, *LAGE-1*, *CT7*, *SCP-1*, *SSX-1*, *SSX-2* and *SSX-4* even after 50 amplification cycles of the 30 brain tumor specimens tested (Fig. 2*a* and Table I). Moreover, the human glioma cell lines and primary-cultured glioma cells did not test positive for any of the 13 CTAs even after 50 amplifica-

TABLE II – INDUCTION OF CTA EXPRESSION BY 5-AZA-CDR IN GLIOMA CELLS AND NORMAL CELLS

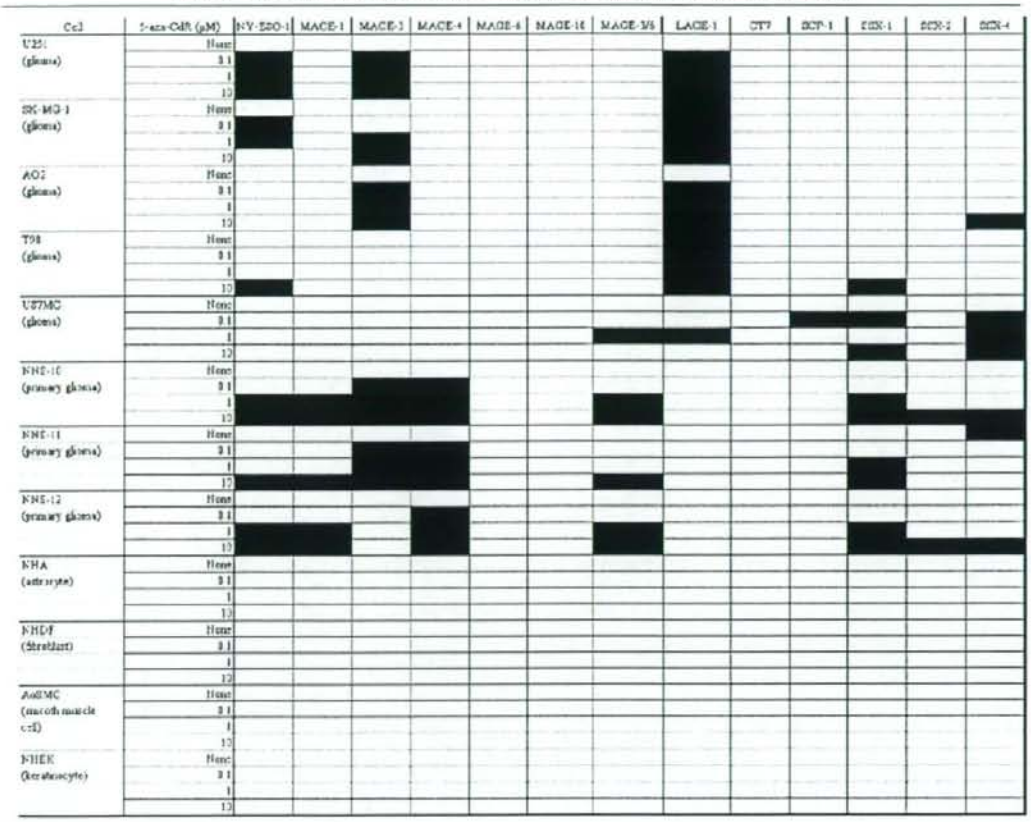

We assessed whether CTAs could be induced by 5-aza-CdR treatment in 5 human glioma cell lines, 3 primary glioma cell lines and 4 human normal cells. The cells were treated with 0.1, 1 and 10 μM 5-aza-CdR every 12 h for 2 consecutive days (4 pulses). The human glioma cell lines and primary-cultured glioma cells did not test positive for any of the 13 CTAs even after 50 amplification cycles. The only exception was *LAGE-1*; SKMG1 and T98 cells constitutively expressed *LAGE-1*. Exposure to 5-aza-CdR invariably induced the expression of *LAGE-1*, *MAGE-1*, *MAGE-3*, *MAGE-4*, *MAGE-3/6*, *SCP-1*, *SSX-1*, *SSX-2*, *SSX-4* and *NY-ESO-1* in CTA-negative glioma cells. Because of toxicity, *NY-ESO-1* expression in SK-MG-1, and *MAGE-3/6* and *LAGE-1* expression in U87MG are not observed when treated with 10 μM 5-aza-CdR. In contrast to glioma cells, administration of the agent does not induce CTA expression in human astrocytes, fibroblasts, smooth muscle cells and epidermal keratinocytes.

tion cycles (Table II). The only exception was *LAGE-1*; SKMG1 and T98 cells constitutively expressed *LAGE-1*.

Effect of 5-aza-CdR on glioma cells and normal human cells in vitro

We assessed whether CTAs could be induced by 5-aza-CdR treatment in 5 human glioma cell lines and 3 primary glioma cell lines. The glioma cells were treated with 0.1, 1 and 10 μM 5-aza-CdR every 12 hr for 2 consecutive days (4 pulses). Table II summarizes the expression of the 13 CTA genes detected by RT-PCR in glioma cell lines treated with 0.1, 1 and 10-μM 5-aza-CdR. Exposure to 5-aza-CdR invariably induced the expression of *LAGE-1*, *MAGE-1*, *MAGE-3*, *MAGE-4*, *MAGE-3/6*, *SCP-1*, *SSX-1*, *SSX-2*, *SSX-4* and *NY-ESO-1* in CTA-negative glioma cells. Among these, we focused on *NY-ESO-1*-the most immunogenic CTA. Real-time quantitative RT-PCR was performed to quantitate *NY-ESO-1* expression in U251, SK-MG-1 and the primary-cultured glioma cells derived from patients (NNS-10, NNS-11 and NNS-12). These results were then compared with those of the *NY-ESO-1*-expressing SaOS-2 cells (Fig. 2*b*). The expression of *NY-ESO-1* was invariably induced by 5-aza-CdR in all glioma cells tested although the efficiency varied among cells; in particular, 10 μM 5-aza-CdR induced toxicity in SK-MG-1, leading to decreased *NY-ESO-1* expression. Similar toxicity occurred in U87MG cells (Table II).

It is particularly important to ensure that CTA is not induced in normal cells, including normal brain cells, in order to prevent them from being targets of CTA-specific immune responses. We therefore treated human astrocytes, fibroblasts, smooth muscle cells and epidermal keratinocytes with 5-aza-CdR. In contrast to